2024 IEEE International Conference on Robotics and Automation (ICRA 2024)
May 13-17, 2024. Yokohama, Japan

Design and Experimental Characterisation of a Novel Quasi-Direct Drive Actuator for Highly Dynamic Robotic Applications

C. Adrián Pérez-Díaz*, Ignacio Muñoz, Daniel Martin-Hernández, Carlos Candelo-Zuluaga, Ivan Torres, Jordi Marsà, Daniel Sanz-Merodio, and Miguel López

***Abstract*— This paper presents the design and experimental results of a proprioceptive, high-bandwidth quasi-direct drive (QDD) actuator for highly dynamic robotic applications. A comprehensive review of the mechanical design of the PULSE115-60 actuator is presented, with particular focus on the design parameters affecting the dynamic performance of the actuator and a full specification is provided. Fundamental parameters to describe the dynamic behaviour of an actuator are discussed, and an experimental method to determine speed and torque bandwidth of the actuator is presented. A rigorous method to determine backdrive torque is also explained. Finally, experimental results quantifying the dynamic performance of the PULSE115-60 actuator are discussed. The PULSE115-60 actuator has a highly dynamic response, surpassing the torque bandwidth at low torque amplitudes showcased in state-of-the-art literature. The differences between current and torque bandwidth, two concepts often conflated in literature, are elucidated. Experimental procedures detailed in previous work are discussed and a novel standardised procedure is proposed for robust characterisation and fair comparison of different actuation systems. Finally, performance results for PULSE115-60 are presented, demonstrating a torque bandwidth of 66.3 Hz at an amplitude of 6 N·m, $\pm 0.11^{\circ}$ of backlash and 0.37 N·m of backdrive torque.**

***Index Terms*— Actuation and Joint Mechanisms, Dynamics, Force Control, Bandwidth, Backdrivability, Transparency, Proprioception, Quasi-Direct Drive, Development and Prototyping, Physical Human-Robot Interaction**

I. Introduction

Robot designers often face the difficult problem of deciding whether to enhance the payload capacity of a robotic system or maximise its dynamic performance. Two main contributors are to blame for this design conundrum: actuators (joints) and links.

Developing an actuator can be difficult since optimising the design to maximise one performance parameter will adversely affect others, forcing the designer to compromise. For example, a direct or quasi-direct drive approach (using actuators with low or no gear ratio) would provide higher bandwidth and minimise the reflected inertia of rotary bodies and friction at the expense of the maximum output torque of the actuators and therefore mass specific torque (torque to mass ratio) [1],[2],[3]. On the other hand, actuators with a high gear ratio (harmonic, cycloidal, etc.) would certainly provide a greater torque to weight ratio and a reduced transmission backlash, at the expense of dynamic performance; impact absorption [4], acceleration, bandwidth and friction among others [5],[6].

The growing demand for robotic solutions for physical Human-Robot Interaction (pHRI) has increased the need for highly dynamic performance whilst ensuring an inherently safe operation [7]. This can be achieved purely through the mechanical design, using decoupling systems or load-dependent and compliant mechanisms [8]; or through an integral design philosophy where low inertia [9], high bandwidth and proprioception are the main drivers for the actuator design. This design paradigm requires a deep re-evaluation of the design/selection choices for all the components of an actuator, analysing the impact of each one on efficiency, bandwidth and proprioceptive performance.

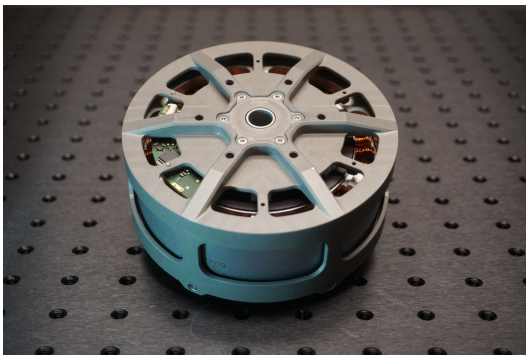

Fig. 1: Prototype of the PULSE115-60 actuator

In this paper, the PULSE115-60 actuator , shown in Fig. 1, is introduced as a first iteration following the QDD design paradigm. Its design was performed from scratch to provide outstanding dynamic response and proprioception capabilities. In order to do so, a new electric motor (P100A) has been developed with the objective of maximising torque per watt and kilogram while operating at low speeds, and high speed and torque bandwidth values. A new 5:1 transmission has been also designed with the aim of reducing rotational inertia and backlash for the specified operational envelope. In the same way, a novel high stiffness torque sensor has been developed and integrated within the actuator, to provide an accurate measurement of both internal and external torques. The low gear ratio also provides the possibility of estimating torque through current [10]. Two absolute, multi-turn encoders have been integrated to provide angular position, velocity and acceleration measurements for both the motor and the output of the actuator.

ARC Robotics, *Arquimea Research Center*, Edificio NANOTEC, Parque Las Mantecas, Cmo de las Mantecas, S/N, 38320 La Laguna, Santa Cruz de Tenerife, Spain. {cperez, imunoz, lmartin, ccandelo, ijtorres, jmarsa, dsanz, mlopez}@arquimea.com

PULSE115-60's performance specifications, obtained from analytical and experimental characterisation, are shown in Table I.

Rated Torque	18.5 N·m @ 48VDC
Peak Torque	62.5 N·m @ 48VDC
Backdrive Torque	0.37 N·m
Transmission Type	Planetary
Gear Ratio	5:1
Backlash	± 0.11 *deg*
Max. Speed @ Rated Torque	90 rpm @ 48VDC
Max. Speed @ Peak Torque	36 rpm @ 48VDC
Mass	1.250 kg
Outer Diameter	113.8 mm
Width	64.2 mm
Hollow Shaft Diameter	10 mm
Rated Current	3.62 A
Peak Current	14.00 A
Voltage Bus	48 V
Rated Electric Power	170 W
Max. Electric Power	235 W
Mass Specific Torque	50 N·m/kg
Generalised Rated Torque Density	13.81 N·m/(A·kg)
Generalised Peak Torque Density	3.57 N·m/(A·kg)
Speed Bandwidth	87.4 Hz @100 rpm, 24VDC
Torque Bandwidth	66.3 Hz @ 6 N·m, 24VDC
Encoder	2x (20 bit) @ Input/Output
Hall Sensor	3x
Thermal Sensor	5x
Capacitive Torque Sensor	1x w/ 1DOF

TABLE I: PULSE115-60 Actuator Specification

II. Mechanical Design

The PULSE115-60 was designed to perform torque and speed profiles within the limits displayed in Table I. The peak torque and maximum speed values were defined according to dynamic requirements extracted from bio-mechanic studies of a human hip [11].

In order to achieve the desired performance, the design aimed to maximise torsional stiffness and minimise inertia of the mechanical transmission (also known as drivetrain), inertia of the structural components and viscous damping. [12]. The transmission gear ratio is another design parameter which has a significant effect on the dynamic performance due to its influence over reflected parameters at the output [2], hence the selection of a low gear ratio. The following equations show the relationship between the previously mentioned parameters:

$$K_T = \sum_{n=1}^{N} \frac{K_n}{i_n^2} \tag{1}$$

$$B_T = \sum_{n=1}^{N} \frac{B_n}{i_n^2} \tag{2}$$

$$J_T = \sum_{n=1}^{N} \frac{J_n}{i_n^2} \tag{3}$$

Where K_T, B_T, J_T, are torsional stiffness, viscous damping, and rotational inertia of the whole system evaluated at the output respectively, and i_n is the transmission ratio of each sub-system [12]. The connections and interactions between each sub-system are considered in the calculations.

The torsional stiffness for metallic structure actuators is usually not considered, since the effect of deformations of the structural components are considered negligible compared to the inertial and damping terms from a system response point of view.

However, depending on the actuator architecture and/or the overall transmission ratio, this term can become significant. Therefore, actuator designers should take into account these parameters and optimise them for a specific use case [2].

In order to facilitate optimisation, an actuator can be understood as a set of sub-systems with multiple interfaces between them: structural, electric motor, drivetrain, power electronics, control electronics and sensing, as shown in Figs. 2 and 3. The design of each sub-system must take into account not only its individual performance but also the interfaces with other sub-systems to achieve the desired system operation. For this reason mechanical and electro-mechanical systems including a new capacitive torque sensor (CTS) integrated in the PULSE115-60 actuator were designed from scratch, to achieve the target performance.

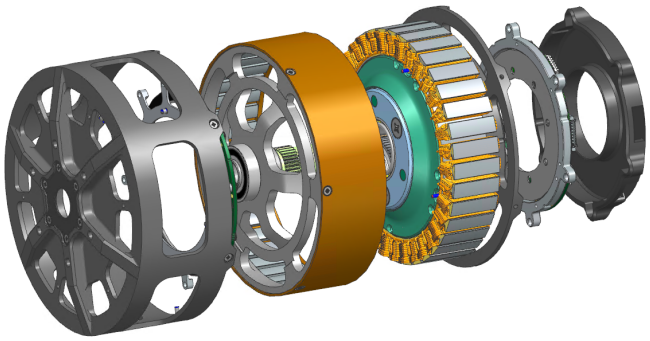

Fig. 2: PULSE115-60 Exploded View

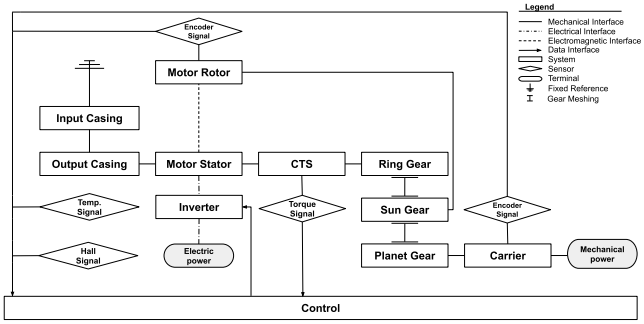

Fig. 3: PULSE115-60 Systems Diagram

A. *Structural Design*

The structural sub-system is comprised of four different assemblies: a first structure, considered fixed; and three structures which transmit the rotary motion of the motor to the actuator output shaft.

The fixed structure is responsible for withstanding all the loads generated by the actuator and reactions caused by the environment. The structure is composed of a two part housing. One of these parts (input housing) is rigidly attached to an upstream body through the actuator mounting interface. The second part (output housing) is fixed to the first to enclose the remaining sub-systems of the actuator. The output housing is the component onto which the CTS and the motor stator are attached.

The torque sensor is rigidly attached to the output structure and is capable of measuring sub-micron structural deformations to infer a torque value. All torque is transmitted through the mechanical interfaces to the torque sensor.

As mentioned earlier, the actuator was designed to minimise mass while maximising the torsional stiffness at the output, optimising the total bandwidth of the system. However, some torsional deformation is necessary for the torque sensor to be able to measure accurately. Thus, a compromise must be made between the overall torsional stiffness and the proprioceptive capability provided by an integrated torque sensor.

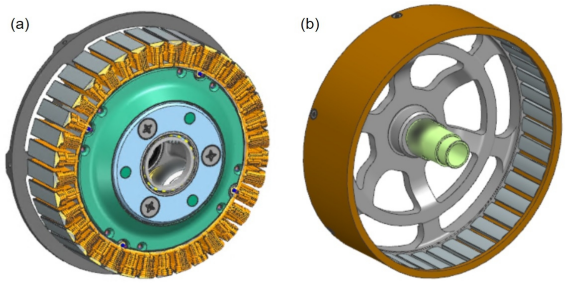

Fig. 4: Motor Stator with Integrated Geared Transmission (a), Motor Rotor Attached to Sun Gear (b)

The first rotating sub-assembly, composed of the rotor, motor magnets, rotor connector and sun gear, is supported by two precision bearings. The rotor connector is rigidly attached to the rotor of the motor and to the axially concentric sun gear as shown in Fig. 4b.

The planet gear sub-assembly, the second rotating structure, is supported radially by a needle bearing and axially by two thrust bearings that reduce friction and consequently damping, increasing backdrivability.

The remaining rotating structure is composed of the carrier and the counter carrier, supported with two ball bearings and connected by the planet gear shafts. The whole assembly is locked axially by means of three screws.

B. *Electric Motor*

The mechanical power of electromagnetic rotary actuators is commonly provided by high-speed/low-torque electric motors. These actuators require the integration of a mechanical transmission with a high reduction ratio to adapt the mechanical power to the application requirements. Designs based on this criteria display high precision and high mass specific torque, however, system responsiveness and proprioceptiveness are drastically reduced, among other performance losses.

PULSE115-60 is equipped with a tailor-made outrunner 3-Phase PMSM electric motor (P100A), designed to provide high toque at low speed. Table II displays its main specifications. Electric motors designed according to this paradigm are known as torque motors. Integrating these motors in actuators allows for low transmission ratios, lowering the reflected inertia and damping, resulting again in increased bandwidth.

DC Bus Voltage	48.00 V
Rated Current	3.65 A
Stall Current	14.00 A
Rated Torque	3.70 N·m
Stall Torque	12.50 N·m @ 48V DC BUS
Rated Torque Constant (K_{Tr})	1.00 N·m/A
Stall Torque Constant (K_{Ts})	0.90 N·m/A
Rated Speed	445 rpm
Max. Speed	500 rpm
Mass (Frameless)	590g
Volume Specific Torque	144.00 kN/m^3 @ Stall
Mass Specific Torque	14.70 N·m/kg @ Stall
Efficiency	79.00 % @ Rated

TABLE II: P100A Motor Specification

C. *Drivetrain*

Robotic platform operation can be divided into two types: non-contact and contact. Non-contact operations (e.g. performing tasks such as spray painting or welding) are extensively utilised and can be widely found in industry. The mechanical design of these kinds of robots requires highly rigid links and high ratio transmissions, facilitating precise and repeatable positioning [13]. In the same way, one of the challenges in robotics is achieving high mass specific torque [2], however this design approach harms dynamic response since the platform loses impact mitigation capability and system responsiveness, and therefore, torque and speed bandwidth. These parameters are crucial for pHRI and mobile robotics, thus, high mass specific torque actuators may perform worse in dynamic applications.

The PULSE115-60 transmission was designed targeting low inertia and low backlash while minimising torque ripple. Moreover, backlash is a non-linearity that may considerably affect the actuator's control and mechanical performance [14], hence decreasing its bandwidth. Besides, backlash magnitude varies with temperature, lubrication, load and transmission and gear meshing configuration, where each individual gear meshing state combines to produce a different backlash magnitude. The transmission was also designed to have reduced peak-to-peak transmission error (PPTE) [15] which reduces torque signal noise and enhances torque bandwidth when the signal is used in the control loop.

As shown in Fig. 3 the actuator's drive train is composed of the electric motor fed by a DC power supply connected to a an electric inverter that delivers the electrical signal defined by the control output to the electric motor's stator, which converts the electrical power into mechanical power to the

rotor. This mechanical power is then directly transferred to an epicyclic planetary transmission with a 5:1 gear ratio and, consequently, to the actuator's mechanical output interface. The transmission is fitted inside the motor stator bore, allowing for a compact actuator assembly. Geared planetary transmissions have showcased superior performance compared to other transmissions, such as strain wave drives, in backdrivability, efficiency and associated motor current consumption [16].

D. *Capacitive Torque Sensor*

Proprioceptive and high bandwidth actuators require integrated force-feedback sensors among others. Capacitive technology has showcased better performance when compared with strain gauges in robotics applications for measuring mechanical displacements to infer torque [17].

The actuator is equipped with an integrated capacitive torque sensor, with high torsional stiffness to enhance bandwidth, where measured torque is inferred from capacitance changes. Results presented in Fig. 5 show how the actuator is capable of sensing a wide range of torques. Displayed data have not been treated or post-processed and future work will aim to improve the sensor's performance.

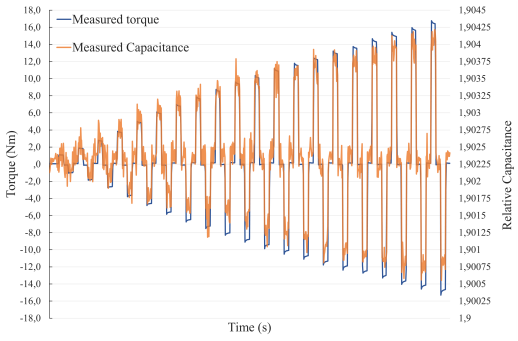

Fig. 5: Measured Torques with Integrated Capacitive Torque Sensor

III. Control and Bandwidth Experiments

The precise measurement of bandwidth and backdrive torque and their use as indicators of dynamic performance in actuators is a subject that has not been rigorously investigated in modern robotics. This section presents the implementation of an actuator control scheme, and details the experiments conducted to determine the bandwidth and backdrive torque of the presented actuator.

A. *Backdrive Torque Experiment*

The backdrive torque is defined as the minimum torque required at the output to overcome the actuator's internal mechanical impedance and initiate the electric motor's rotor movement. It quantifies the ability of an actuator to be driven from the load side. Low backdrive torque actuators are essential for developing human-centred robotic devices.

To characterise the backdrivability of the PULSE115-60 actuator, the output shaft was moved with an external motor, providing a sinusoidal speed signal with a frequency of 1 to 2 Hz, and the actuator motor phases left in open circuit. Previous studies detail methods for measuring backdrive torque. One such method defines the backdrive torque as the torque applied at which the output reaches a particular angular velocity [18]. The angular velocity is selected somewhat arbitrarily and therefore does not give a robust and reliable measure of backdrive torque, making meaningful comparison between actuators difficult.

In this paper, a rigorous approach is proposed for experimentally determining the backdrive torque of a rotary actuator. The angle at the input and output of the actuator are measured, and the ratio between their respective angular velocities are calculated. Since the actuator is not backlash-free, the backdrive torque is defined as the torque at which the ratio between the velocities recorded by the input and output encoders converges within $\pm 1\%$ error of the design value (5:1). This criterion also takes into account transmission error inherent in geared drives.

B. *Speed and Torque Control*

This section presents the Field-Oriented Control (FOC) scheme which manages the P100A electric motor integrated in the PULSE115-60 actuator. Fig. 6 depicts the speed and torque control schemes implemented and used in the experiments to determine the actuator's bandwidth response.

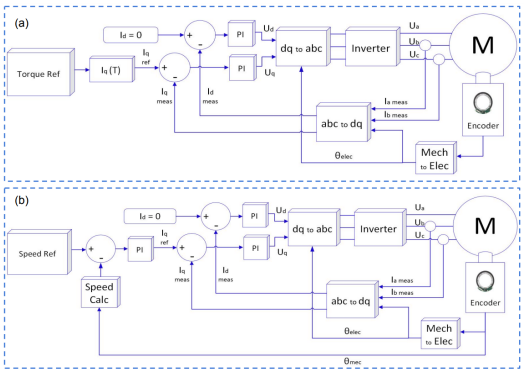

Fig. 6: Torque Control (a) and Speed Control (b) Schemes Based on Field Oriented Control (FOC)

C. *Bandwidth Calculation Experiments*

Previous works present different criteria for defining the torque bandwidth of an actuator. When measuring the bandwidth of mechanical systems, the influence of the implemented control should be taken into account.

For instance, when a current control loop is nested in a torque loop [19], the torque bandwidth is one order of magnitude lower when compared against a standalone current loop inferring the transmitted torque from the current measurement [2]. Additionally, when a standalone current loop is used, if instead of being inferred the torque is measured by a transducer and fed back, a delay is included due to the intrinsic bandwidth of the torque sensor, decreasing torque bandwidth.

This paper presents a standalone current loop scheme, with a torque transducer at the actuator output, used only for bandwidth measurement as shown in 6 (a). This configuration is chosen because the measurement of bandwidth will include the lag time effects of the whole mechanical system, which are not taken into account using other methods. This measurement method allows for more realistic comparison between actuator designs.

In addition, many of the experiments described in literature estimate bandwidth from the response to a step stimulus [18],[2]. Although it theoretically provides an adequate value for the bandwidth, great precision in measurements is necessary to obtain it accurately. Furthermore, calculating the bandwidth of an actuator with a step-response experiment is unreliable due to the inherent non-linear effect of backlash which significantly influences the achievable bandwidth during reversing torque operation.

The stimulus for a robust characterisation of bandwidth in this type of transmission must include changes in the direction of movement, for example, a sinusoidal signal. In reference [20], a method to measure torque bandwidth in electric rotary actuators is presented. A set of experiments is conducted to obtain the bandwidth of the actuator's response based on a set of constant amplitude chirp signals.

Fig. 7 presents a schematic layout of the test bench designed for the experiments, Fig. 8 shows the finished mechanical assembly. A SpeedGoat real-time target machine provides the capacity to carry out the control presented in the previous section while collecting the experimental data.

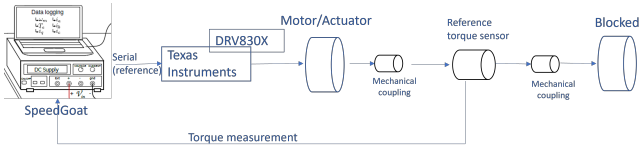

Fig. 7: Test Bench Utilised in the Characterisation Experiments

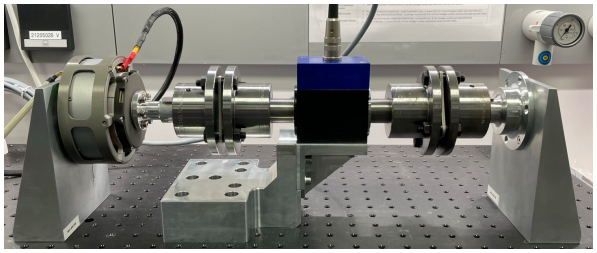

Fig. 8: Torque Bandwidth Experimental Setup

In order to establish the bandwidth of the actuator, the experimental procedure followed is similar to the one outlined in reference [20]. The actuator is excited with a sine wave signal of fixed amplitude. Over time, the signal frequency is increased in discrete steps. At each frequency, the response of the actuator is measured. The actuator's attenuation and phase shift in response to the reference signal are calculated at each frequency. The actuator bandwidth corresponds to either the frequency at which the response is attenuated below -3dB or the frequency at which the phase shift exceeds 180º.

The rotor shaft is mechanically fixed for the torque experiments while left unrestricted for speed experiments.

A tuning process is used to find an appropriate combination of control constants K_p and K_i. The procedure starts by determining the theoretical constants based on the physical characteristics of the actuator, similar to the process in reference [22], subsequently an algorithm performs a sweep to test multiple combinations of K_p and K_i to find the best torque bandwidth.

D. *Experimental Results and Data Analysis*

Although speed and torque bandwidth are intrinsically related, the benefits of either torque or speed bandwidth will be exploited depending on the application. For example, a wide speed bandwidth is necessary in drone flight control systems and target tracking systems, while in industrial robotic arms and rehabilitation robots, torque bandwidth takes precedence.

*1) **Backdrivability Experiments**:* Backdrive torque of the PULSE115-60 actuator is measured using the experimental method specified in Section III-A, resulting in a value of 0.37 N·m.

Figure 9 shows the backdrive torque measurements for 4 out of the 15 different output angular positions evaluated, spread evenly over one full output rotation. The backdrive torque was calculated as the mean value of the data points obtained. Consequently, different gear meshing configuration effects were taken into account, including backlash and transmission error variation during the whole rotation.

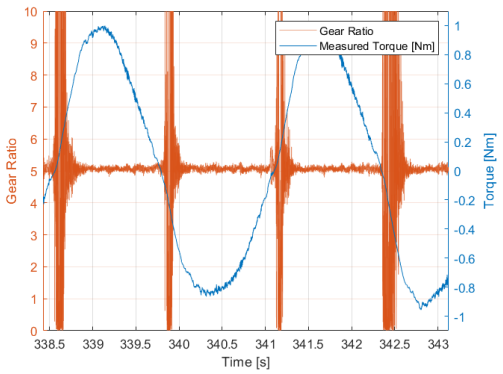

Fig. 9: PULSE115-60 Backdrive Torque Experiment Data

*2) **Speed Bandwidth Experiments**:* The experimental measurements demonstrate that a speed bandwidth of 87.4 Hz at an amplitude of 100 rpm is achieved, comparable to what is found in the literature, which reports a bandwidth of 5 Hz at an amplitude of 500 rpm [23]. Fig. 10 shows the sweep results of the constants Kp and Ki used in the speed PID loop and the bandwidth achieved.

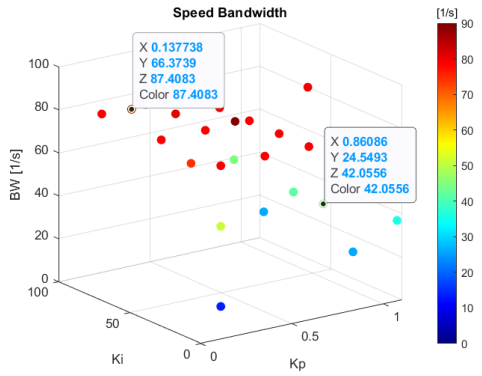

Fig. 10: PULSE115-60 Speed Bandwidth vs Kp and Ki with an Amplitude of 100 rpm

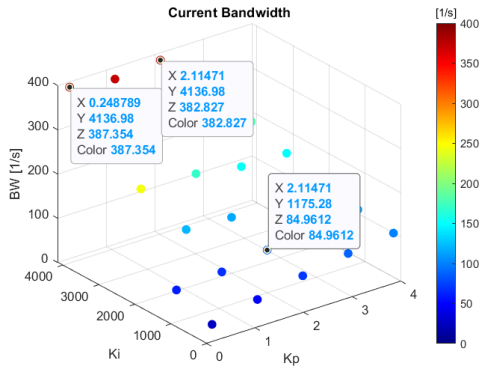

Fig. 12: PULSE115-60 Current Bandwidth vs Kp and Ki with an Amplitude of 0.6 A

*3) **Torque and Current Bandwidth Experiments**:* To demonstrate the difference between current control loop bandwidth and torque bandwidth, both values were obtained from the same experimental setup and run.

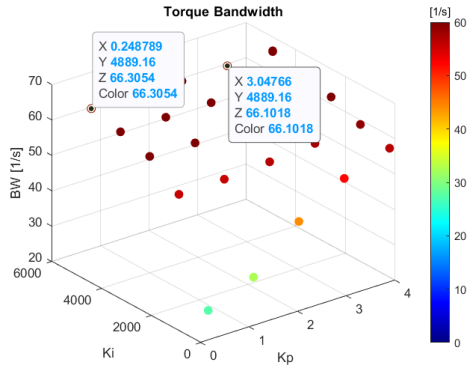

Fig. 11: PULSE115-60 Torque Bandwidth vs Torque Kp and Ki with an Amplitude of 6 N·m

PULSE115-60 achieves a torque bandwidth of 66.3 Hz at an amplitude of 6 N·m as shown in Fig.11, while, a current bandwidth of 387 Hz is measured in the same experiment as shown in Fig. 12. These measurements show the importance of including the lag time effects of the whole mechanical system to enable realistic comparison between actuator designs.

Table III compares the dynamic characteristics of the most commonly used actuators in robotics. It is worth mentioning that the PULSE115-60 actuator reaches a bandwidth comparable to the QDD actuator results presented in reference [1].

Nevertheless, it remains unclear if the bandwidth values are truly comparable since the experimental procedure presented by Yu et al. [1] does not specify if the value measured represents actual torque bandwidth or current loop bandwidth as explained earlier.

IV. Conclusions

In conclusion, this paper introduces PULSE115-60, the first iteration of a new QDD actuator design with proprioceptive capabilities, and enhanced dynamic bandwidth and backdrivability.

A new set of experimental procedures are proposed to characterise bandwidth and backdrivability in a repeatable and accurate manner. Discussion clarifying the distinction between torque and current bandwidth has been also presented, highlighting that toque bandwidth is a more robust and pragmatic measure of actuator dynamic response.

Finally, the results obtained demonstrate how the PULSE115-60 actuator design showcases excellent backdrivability and bandwidth performance when compared popular commercial actuators and state-of-the-art results available in literature. However, effective comparison is hindered by inconsistent and obscure measurement procedures.

ACKNOWLEDGEMENT

Funded by the European Union. Views and opinions expressed are however those of the author(s) only and do not necessarily reflect those of the European Union. Neither the European Union nor the granting authority can be held responsible for them.

Parameter	EC45/HD[1]	EC90/HD[1]	Yu et al.[1]	HEBI X8-16[21]	PULSE115-60
Peak Torque [N·m]	8	40	17.5	34.0	62.5
Actuator Mass [kg]	0.5	1.8	0.77	0.49	1.25
Mass Specific Torque [N·m/kg]	16	22.2	20.7	77.6	50
Torque Bandwidth [Hz]	5.1 @ 5 N·m	4.2 @ 5 N·m	62.4 @ 10 N·m	19 @ 4 N·m	66.3 @ 6 N·m
Backdrive Torque [N·m]	2.88	6.1	0.97	-	0.37
Tansmission Ratio	50:1	100:1	8:1	1462.2 : 1	5:1

TABLE III: Actuator Dynamics Comparison

REFERENCES

[1] S. Yu, T.-H. Huang, X. Yang, C. Jiao, J. Yang, Y. Chen, J. Yi, and H. Su, "Quasi-direct drive actuation for a lightweight hip exoskeleton with high backdrivability and high bandwidth," *IEEE/ASME Transactions on Mechatronics*, vol. 25, no. 4, pp. 1794–1802, 2020.

[2] P. M. Wensing, A. Wang, S. Seok, D. Otten, J. Lang, and S. Kim, "Proprioceptive actuator design in the mit cheetah: Impact mitigation and high-bandwidth physical interaction for dynamic legged robots," *Ieee transactions on robotics*, vol. 33, no. 3, pp. 509–522, 2017.

[3] A. Singh, N. Kashiri, and N. Tsagarakis, *Design of a Quasi-Direct-Drive Actuator for Dynamic Motions*, Nov. 2020, vol. 64, journal Abbreviation: Proceedings Publication Title: Proceedings.

[4] C. Relaño, D. Sanz-Merodio, M. Lopez, and C. Monje, "Generalization of impact response factors for proprioceptive collaborative robots," in *Proceedings. 2023 IEEE International Conference on Robotics and Automation*. IEEE, 2023.

[5] E. Dunwoodie, R. Mutlu, B. Ugurlu, M. Yildirim, T. Uzunovic, and E. Sariyildiz, "A High-Torque Density Compliant Actuator Design for Physical Robot Environment Interaction," in *2020 IEEE 16th International Workshop on Advanced Motion Control (AMC)*, Sep. 2020, pp. 1–6, iSSN: 1943-6580.

[6] Q. Hua, W. Zhou, S. Zhu, Y. Yao, C. Cheng, A. Xie, and D. Zhang, "Design of a high-torque robot joint and its control system," *Journal of Physics: Conference Series*, vol. 2281, no. 1, p. 012007, jun 2022. [Online]. Available: https://dx.doi.org/10.1088/1742-6596/2281/1/012007

[7] H. Lee, B. Lee, W. Kim, M. Gil, J. Han, and C. Han, "Human-robot cooperative control based on pHRI (Physical Human-Robot Interaction) of exoskeleton robot for a human upper extremity," *International Journal of Precision Engineering and Manufacturing*, vol. 13, no. 6, pp. 985–992, Jun. 2012. [Online]. Available: https://doi.org/10.1007/s12541-012-0128-x

[8] E. Saerens, R. G. Furnémont, J. Legrand, S. Crispel, P. Lopez Garcia, T. Verstraten, B. Vanderborght, and D. Lefeber, "Novel specta actuator to improve energy recuperation and efficiency," *Actuators*, vol. 11, no. 3, p. 64, Feb 2022. [Online]. Available: http://dx.doi.org/10.3390/act11030064

[9] K. Urs, C. E. Adu, E. J. Rouse, and T. Y. Moore, "Alternative metrics to select motors for quasi-direct drive actuators," 2022.

[10] H. Xiang, K. Xiang, Y. Fang, M. Pang, B. Tang, J. Luo, and G. Zhu, "Torque estimation base on quasi-direct drive actuators," pp. 1637–1642, 2022.

[11] K. Embry, "The Effect of Walking Incline and Speed on Human Leg Kinematics, Kinetics, and EMG," Oct. 2018. [Online]. Available: https://ieee-dataport.org/open-access/effect-walking-incline-and-speed-human-leg-kinematics-kinetics-and-emg

[12] P. Lopez Garcia, E. Saerens, S. Crispel, A. Varadharajan, D. Lefeber, and T. Verstraten, "Factors influencing actuator's backdrivability in human-centered robotics," *MATEC Web of Conferences*, vol. 366, p. 01002, 2022. [Online]. Available: https://www.matec-conferences.org/10.1051/matecconf/202236601002

[13] B. Eberman and J. Jr, "Whole-arm manipulation: Kinematics and control," p. 8, 03 1995.

[14] S. Habibi, J. Roach, and G. Luecke, "Inner-Loop Control for Electromechanical (EMA) Flight Surface Actuation Systems," *Journal of Dynamic Systems, Measurement, and Control*, vol. 130, no. 5, p. 051002, 08 2008. [Online]. Available: https://doi.org/10.1115/1.2936382

[15] O. Mohammed, "A study of different considerations to meet gear design requirements," *Procedia Structural Integrity*, vol. 42, pp. 1607–1618, 12 2022.

[16] M. J. Nandor, M. Heebner, R. Quinn, R. J. Triolo, and N. S. Makowski, "Transmission comparison for cooperative robotic applications," vol. 10, no. 9. [Online]. Available: https://www.mdpi.com/2076-0825/10/9/203

[17] M. Y. Cao, S. Laws, and F. R. y. Baena, "Six-axis force/torque sensors for robotics applications: A review," *IEEE Sensors Journal*, vol. 21, no. 24, pp. 27 238–27 251, 2021.

[18] H. Zhu, C. Nesler, N. Divekar, M. Ahmad, and R. Gregg, "Design and Validation of a Partial-Assist Knee Orthosis with Compact, Backdrivable Actuation," vol. 2019, Jun. 2019, pp. 917–924.

[19] T. Zhang and H. Huang, "A Lower-Back Robotic Exoskeleton: Industrial Handling Augmentation Used to Provide Spinal Support," *IEEE Robotics & Automation Magazine*, vol. 25, no. 2, pp. 95–106, Jun. 2018. [Online]. Available: https://ieeexplore.ieee.org/document/8360955/

[20] J. Malzahn, N. Kashiri, W. Roozing, N. Tsagarakis, and D. Caldwell, "What is the torque bandwidth of this actuator?" in *2017 IEEE/RSJ International Conference on Intelligent Robots and Systems (IROS)*. Vancouver, BC: IEEE, Sep. 2017, pp. 4762–4768. [Online]. Available: http://ieeexplore.ieee.org/document/8206351/

[21] I. P. HEBI Robotics, "Hebi robotics: Documentation." [Online]. Available: https://docs.hebi.us/hardware.htmlx-series-actuators

[22] M. Găiceanu, "Advanced Control of the Permanent Magnet Synchronous Motor," in *Electric Machines for Smart Grids Applications - Design, Simulation and Control*, A. El-Shahat, Ed. IntechOpen, Dec. 2018.

[23] Y. Li, X. Guan, X. Han, Z. Tang, K. Meng, Z. Shi, B. Penzlin, Y. Yang, J. Ren, Z. Yang, Z. Li, S. Leonhardt, and L. Ji, "Design and Preliminary Validation of a Lower Limb Exoskeleton With Compact and Modular Actuation," *IEEE Access*, vol. 8, pp. 66 338–66 352, 2020. [Online]. Available: https://ieeexplore.ieee.org/document/9057535/